Buckling Instability in Growing Tumor Spheroids

P. Ciarletta

Phys. Rev. Lett. **110**, 158102 — Published 9 April 2013

DOI: 10.1103/PhysRevLett.110.158102

Buckling instability in growing tumor spheroids

P. Ciarletta[1,2*]
[1] *CNRS and Institut Jean le Rond d'Alembert, UMR 7190, Université Paris 6, 4 place Jussieu case 162, 75005 Paris, France*
[2] *MOX - Politecnico di Milano and Fondazione CEN, piazza Leonardo da Vinci 32, 20133 Milano, Italy*

A growing tumor is subjected to intrinsic physical forces, arising from the cellular turnover in a spatially constrained environment. This work demonstrates that such residual solid stresses can provoke a buckling instability in heterogeneous tumor spheroids. The growth rate ratio between the outer shell of proliferative cells and the inner necrotic core is the control parameter of this instability. The buckled morphology is found to depend both on the elastic and the geometric properties of the tumor components, suggesting a key role of residual stresses for promoting tumor invasiveness.

PACS numbers: 46.32.+x, 87.10.Pq

The evolution of living matter, from bacteria to high-level eukaryotic systems, is strongly influenced by the physical and mechanical characteristics of the micro-environment. In fact, cells respond not only to soluble biochemical signals but also to physical factors, through surface receptors. Applied forces are sensed by integrins and focal adhesion proteins, and transformed into a chemical activity which, in turn, activates actomyosin contractility for establishing a balance between endogenous and exogenous forces, also known as tensional homeostasis [1]. Such a mechanical feedback plays a key role in many physiological processes, e.g. allowing cell spreading to adapt to the substrate stiffness by modulating the pulling force [2], or regulating cell growth, differentiation and tissue development during morphogenesis [3]. Nevertheless, a loss of tensional homeostasis is often considered as a hallmark of disease. This happens, for example, in cancer development, whereby the healthy extra-cellular matrix is initially remodeled into a stiffer desmoplastic stroma, provoking an altered homeostatic tension which drives the genetic expression of a malignant phenotype [4]. Such a pathological remodeling explains why tumor screening often resides on palpation techniques to detect a stiff mass within a soft tissue. Physical forces are equally determinant in metastasis, modulating cell migration towards the blood vessels [5] and directing intravasation and extravasation processes in the vascular system [6]. Recent theoretical studies have demonstrated that the cell-cell and cell-matrix interactions, mediated by cadherins and integrins, respectively, may drive the morphological patterns of invasive tumors [7, 8]. Furthermore, a growing tumor is also subjected to intrinsic forces, arising from the cellular turnover in a spatially constrained environment: cell proliferation and programmed death (apoptosis) typically provoke elevated interstitial fluid pressure and solid stress in tumors [9]. Growth-induced solid or residual stress accumulates during tumor progression, possibly driving the collapse of blood and lymphatic vessels, thus making the vascular delivery of anti-cancer drugs ineffective.

Tumor development is driven by a complex interplay between biological processes, biochemical reactions and feedbacks mechanisms with the environment [10]. For instance, cancer cells adapt to both hypoxic conditions and immune system by activating signaling pathways which enforce proliferation and promote angiogenesis [11]. Chemokines and growth factors are known to mediate chemotaxis and trigger directional migration into the stroma, which frequently shape morphological changes of the tumor into a pro-metastatic state [12]. The aim of this work is to explore whether the residual stresses generated by differential growth processes can also be involved

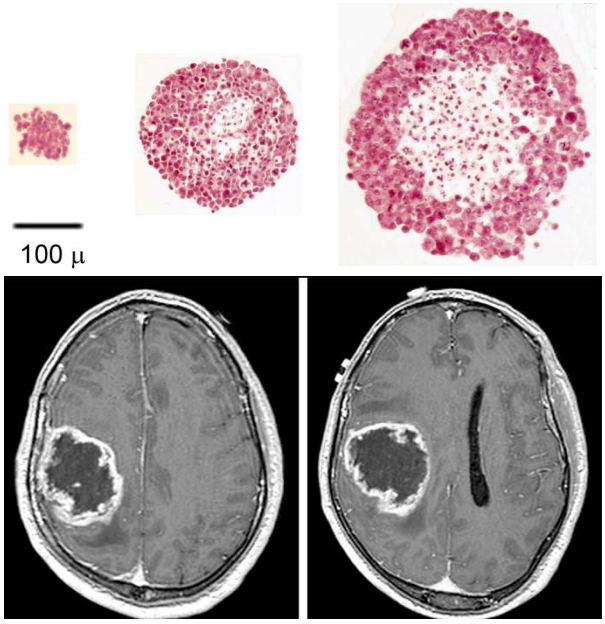

FIG. 1. (color online). Morphological evolution of a multicellular tumor spheroid of HeLa cells, developing an undulated contour and a necrotic core (lighter cells). The bar is 100 μm (top, from [16]). Magnetic Resonance sections of a glioblastoma multiforme, an irregular brain tumor characterized by the presence of inner necrosis (bottom).

into the formation of protrusions in tumor spheroids. A similar mechanism has been invoked to reproduce the pattern development in algae [13], in monolayered epithelia [14] and in tubular tissues [15]. The loss of circularity of the tumor is related to the development of an inner nucleus of necrotic cells, *due to local hypoxia*, whilst tumor cell proliferation is restricted to an outer rim. This morphological change is depicted in Fig. 1 for both a freely expanding multi-cellular tumor spheroid (MCTS) *in vitro* and a glioblastoma multiforme *in vivo*. Several experimental techniques have been proposed for modeling cancer cells at different scales (see [17] for a review), showing that tumor spheroids behave as elasto-visco-plastic solids, with a shear modulus and a dynamic viscosity [18]. The spherical symmetry of the system model imposed zero shear stresses, so that the yield stress of cellular plasticity can be neglected in the following. Jain and coworkers have studied the mechanical characteristics of tumor aggregates for more than a decade. In [19], the growth induced solid stress in growing MCTS was estimated in the range 6-16 kPa. In another study, confined compression tests have been performed for different tumor lines, reporting that the stress reached an equilibrium value after a typical relaxation time of few minutes [20]. Nonlinear stress-strain curves at equilibrium have been found, measuring the initial elastic modulus in the range 4-40 kPa. In a more recent work, murine and human tumors have been cut in order to measure the relaxed shape of the excised tumor, so that the residual stresses have been evaluated at about 0.37-8 kPa [9].

The tumor spheroid is modeled as an elastic heterogeneous body initially made of an inner necrotic core and an outer shell of proliferative cells, whose physical fields are indicated in the following with superscripts c and s, respectively. Using the spherical coordinate system, the spatial (resp. material) position vector is indicated by $\mathbf{x}(r,\theta,\phi)$(resp.$\mathbf{X}(R,\Theta,\Phi)$), so that R_i,R_o (resp. r_i,r_o) are the inner and outer radii in the reference (resp. spatial) configuration, and $\mathbf{F}=\partial\mathbf{x}/\partial\mathbf{X}$ is the deformation gradient. In particular, R_i can be considered as the radius of the nucleated necrotic core, that must be about few times the cellular size (e.g. at least $60\mu m$) to respect the continuum hypothesis, whilst R_o is the outer radius of the tumor spheroid at the time when the necrosis begin. This last value has been measured in MCTS within the range $152-516\ \mu m$, reporting a a variability with the change of glucose and oxygen concentrations [21]. Using the classical treatment for volumetric growth in soft materials [22], the multiplicative decomposition $\mathbf{F}=\mathbf{F}_e\mathbf{F}_g$ applies, where $\mathbf{F}_g$ is the growth tensor and $\mathbf{F}_e$ is the elastic counterpart which restores compatibility of the overall deformation. In particular, a homogeneous growth is assumed for both the necrotic core and the outer shell, i.e. $\mathbf{F}_g^k=g_k\mathbf{I}$ with $k=(c,s)$, where $\mathbf{I}$ is the unit matrix and g_c, g_s are the respective isotropic growth rates. This assumption resides on the observation that the characteristic (doubling) time of volumetric growth (days) is much greater than both the viscoelastic time (minutes) and the growth relaxation time for internal dynamic re-organization towards an homeostatic state (minutes)[23]. Recalling that tumor cells are mostly made by water, using the incompressibility constraint and the compatibility condition $r^c(R_i)=r^s(R_i)=g_cR_i$, the elastic displacement fields read $r^c=g_cR^c$ and $(r^s)^3=g_s^3(R^s)^3-(g_s^3-g_c^3)R_i^3$. Accordingly, the elastic deformation tensors can be expressed as $\mathbf{F}_e^c=\mathbf{I}$ and $\mathbf{F}_e^s=\mathrm{diag}(\lambda_{\mathrm{r}}^{\mathrm{s}},\lambda_\theta^{\mathrm{s}},\lambda_\phi^{\mathrm{s}})$, where the principal stretches of the shell read $\lambda_r^s=(g_c/g_s)\partial_R r^s$ and $\lambda_\theta^s=\lambda_\phi^s=(g_c/g_s)r^s/R^s$. In order to take into account the experimental responses in [20], the tumor aggregates are modeled using the equilibrium elastic energy density of the neo-Hookean materials, being:

$$W^k=\mu^k/2({\lambda_r^k}^2+{\lambda_\theta^k}^2+{\lambda_\phi^k}^2-3)+p^k(\lambda_r^k\lambda_\theta^k\lambda_\phi^k-1) \quad (1)$$

where μ^k are the shear moduli and p^k are Lagrangian multipliers, with $k=(c,s)$. From Eq.(1), the Cauchy stress components read ${\sigma^k}_{ij}=(\mu^k{\lambda_i^k}^2-p^k)\delta_{ij}$, where δ_{ij} is the Kronecker delta and (i,j) span over (r,θ,ϕ). In spherical symmetry, the equilibrium equations $\nabla\cdot\boldsymbol{\sigma}^{\mathrm{k}}=0$ simplify as $\partial_r(r^2\sigma_{rr}^k)-r(\sigma_{\theta\theta}^k+\sigma_{\phi\phi}^k)=0$. Using the stress-free boundary condition at the outer surface $\sigma_{rr}^s(r_o)=0$, the residual stress components inside the tumor shell are given by:

$${\sigma^s}_{ii}=\mu^s\left({\lambda_i^s}^2-{\lambda_r^s}^2-2\int_r^{r_o}\frac{{\lambda_\phi^s}^2-{\lambda_r^s}^2}{r}dr\right) \quad (2)$$

Taking into account the normal continuity of the stress fields at the interface between the necrotic core and growing rim, the inner core is subjected to a homogeneous stress state such that ${\sigma^c}_{jj}(r)={\sigma^s}_{rr}(r_i)$, with $j=(r,\theta,\phi)$. In summary, Eq.(2) states that if the volume of the proliferative cells increases more than the necrotic core (i.e. $g_s/g_c>1$), then this differential growth induces a compressive (resp. tensile) residual hoop (resp. radial) stress within the tumor rim. If the hoop stress accumulates above a certain threshold, it is possible that a buckling instability occurs so that the spheroid assumes an undulated morphology.

The theory of incremental displacement superposed on finite elastic deformation can be employed in order to investigate the elastic stability of the tumor spheroid. In particular, indicating with an upper bar the physical fields after perturbation, the position within the tumor mass is taken as $\bar{\mathbf{x}}=\mathbf{x}+\delta\mathbf{x}$, where $\mathbf{x}$ is the spherically symmetric solution and $\delta\mathbf{x}$ is the infinitesimal incremental displacement. Accordingly, since growth is not affected by the perturbation, the first-order expansions of the elastic deformation tensors read $\bar{\mathbf{F}}_e^k=(\mathbf{I}+\delta\mathbf{F}_e^k)\mathbf{F}_e^k$, where $\delta\mathbf{F}_e^k=\partial(\delta\mathbf{x}^k)/\partial\mathbf{x}$ and $k=(c,s)$. Setting $\bar{\boldsymbol{\sigma}}^k=\boldsymbol{\sigma}^k+\delta\boldsymbol{\sigma}^k$, the incremental Cauchy stress components can

be calculated by differentiating Eq.(1) as:

$$\delta\sigma^k_{ij} = L^k_{ijlm}\delta F^k_{ml} + p^k\ \delta F^k_{ij} - \delta p^k\ \delta_{ij} \tag{3}$$

where δp is the incremental Lagrange multiplier, $L^k_{ijlm} = \mu^k\delta_{jm}\delta_{il}(\lambda^k_i)^2$ are the instantaneous elastic moduli, (i,j) span over (r,θ,ϕ) and Einstein's summation rule on repeated subscript indices is assumed.

A general perturbation can be chosen in the form $\delta\mathbf{x}^k = [u^k(r,\theta,\phi), v^k(r,\theta,\phi), w^k(r,\theta,\phi),]^T$, with the incremental displacement fields u^k, v^k, w^k given as functions of the spherical harmonics Y^l_m of order l and degree m. For isotropic materials, the incremental equation for w^k decouples in the boundary value problem [24], and an axisymmetric perturbation can be chosen for the sake of simplicity. Setting $w^k = 0$, the incremental mapping should also be incompressible, imposing that:

$$\partial_r(r\ u) + \partial_\theta v + u + v\ \cot\theta = 0 \tag{4}$$

Moreover, the governing equations are independent on the order l of the spherical harmonics [25]: setting $l = 0$ a functional dependence on the Legendre polynomials $P_m = P_m(\cos\theta)$ of degree m can be considered. In particular, a variable separation is assumed such that $[u^k, \delta\sigma^k_{rr}, \delta p^k]^T = [U^k(r), \Sigma^k_{rr}(r), P^k(r)]^T \cdot P_m$ and $[v^k, \delta\sigma^k_{r\theta}]^T = [V^k(r), \Sigma^k_{r\theta}(r)]^T \cdot \partial_\theta(P_m)/\sqrt{m(m+1)}$. The incremental elastic boundary value problems are given by solving the two independent equilibrium equations $\nabla\cdot\delta\boldsymbol{\sigma}^k = 0$ and the incompressibility condition, given by Eq.(4), for both the outer shell and the necrotic core. Setting $\mathbf{U}^k = [U^k, V^k]^T$ and $\boldsymbol{\Sigma}^k = [\Sigma^k_{rr}, \Sigma^k_{r\theta}]^T$, the stress-free boundary conditions at the outer radius read $\boldsymbol{\Sigma}^s(r_o) = \mathbf{0}$, while the continuity relations of the physical fields at the interface rewrite $\mathbf{U^c}(r_i) = \mathbf{U^s}(r_i)$ and $\boldsymbol{\Sigma}^c(r_i) = \boldsymbol{\Sigma}^s(r_i)$. Recalling that the necrotic core is subjected to a homogeneous deformation, the governing equations can be easily manipulated to be transformed into a forth-order differential equation in U^c. Avoiding singularities at $r = 0$, the analytical solution for the displacements within the necrotic core yields:

$$U^c(r) = \alpha_1 r^{m+1} + \alpha_2 r^{m-1} \tag{5}$$

where α_1 and α_2 are constant parameters, and we must look for solutions with integer values of $m \geq 2$. At $r = r_i$, a functional dependence can be expressed between the displacement and the stress fields, as $r_i^2\boldsymbol{\Sigma}^c(r_i) = \mathbf{Z}^c(r_i)\cdot\mathbf{U}^c(r_i)$, where $\mathbf{Z}^c$ is the surface impedance matrix for the necrotic core.

In order to solve the boundary value problem for the outer tumor shell, it is very helpful to transform the governing equations into the Stroh formalism, adopting a procedure often employed in elastodynamic problems with radial inhomogeneities [26]. In practice, the incremental field δp^s can be eliminated using Eq.(3), so that the governing equations can be recast in the form of a first order differential system. Introducing the displacement-traction vector $\boldsymbol{\eta}^s = [\mathbf{U}^s, r^2\boldsymbol{\Sigma}^s]^T$, the Stroh form of the incremental equations reads:

$$\frac{d\boldsymbol{\eta}^s}{dr} = \mathbf{N}\boldsymbol{\eta}^s = \begin{bmatrix} \mathbf{N}_1 & \mathbf{N}_2 \\ \mathbf{N}_3 & -\mathbf{N}_1^T \end{bmatrix}\boldsymbol{\eta}^s \tag{6}$$

where $\mathbf{N}$ is the so-called *Stroh matrix*, that can be simplified by the means of three 2x2 sub-blocks $\mathbf{N}_1$, $\mathbf{N}_2$ and $\mathbf{N}_3 = \mathbf{N}_3^T$, whose full derivation can be found in the Supplementary Material. Using Eq.(5), the determinant method can be used to find the threshold values g_s/g_c which numerically solve Eq.(6), with the given boundary conditions, fixing the wavenumber m and the initial aspect ratio R_o/R_i [27]. Although effective for thin geometries, such a numerical method can run into stiffness problems for thick shells. Such a limitation can be avoided using another numerical procedure, which is presented in the following. Recalling the boundary condition $\boldsymbol{\Sigma}^s(r_o) = \mathbf{0}$, it is possible to define a functional dependence between the traction and the displacement amplitudes as $r^2\boldsymbol{\Sigma}^s = \mathbf{Z}^s\ \mathbf{U}^s$, where $\mathbf{Z}^s$ is the conditional impedance matrix, with $\mathbf{Z}^s(r_o) = \mathbf{0}$ [28]. Therefore, it is possible to use $\mathbf{Z}^s$ in Eq.(6) for eliminating $\mathbf{U}^s$, so that the incremental elastic problem rewrites as a Riccati differential equation in $\mathbf{Z}^s$, being:

$$\frac{d}{dr}\mathbf{Z}^s = \mathbf{N}_3 - \mathbf{N}_1^T\mathbf{Z}^s - \mathbf{Z}^s\mathbf{N}_1 - \mathbf{Z}^s\mathbf{N}_2\mathbf{Z}^s \tag{7}$$

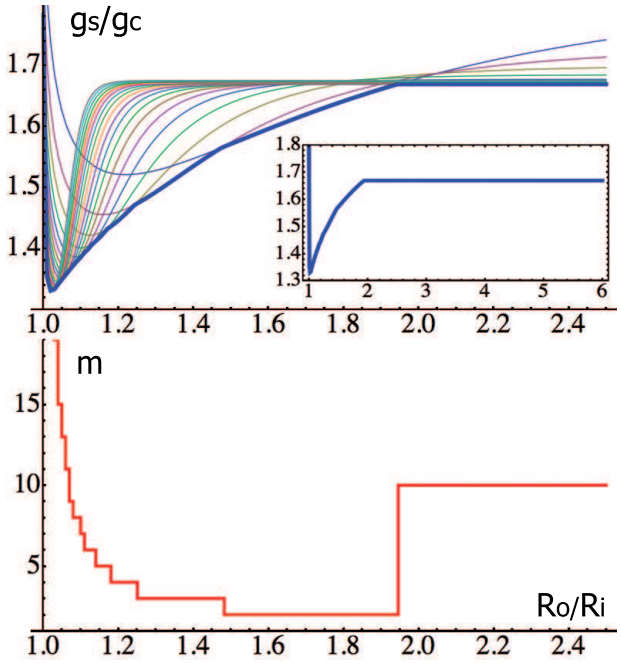

FIG. 2. (color online). Marginal stability curves for g_s/g_c (top, thick line) and m (bottom) versus the aspect ratio R_o/R_i, calculated for $\mu^s/\mu^c = 1$. The thin solid lines represent the critical thresholds g_s/g_c for different values of the wavenumber $m = 2, .., 20$. Inset: marginal stability curve for g_s/g_c versus a larger range of R_o/R_i.

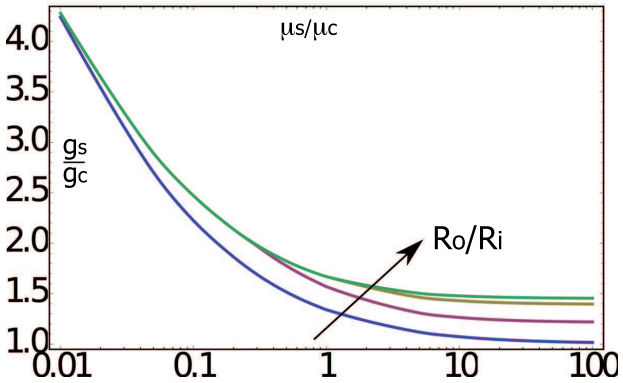

FIG. 3. (color online). Logarithmic plot of the marginal stability curves for g_s/g_c versus the shear moduli ratio μ^s/μ^c. The solid lines represent the instability thresholds for $R_o/R_i = 1.05, 1.5, 2, 3$.

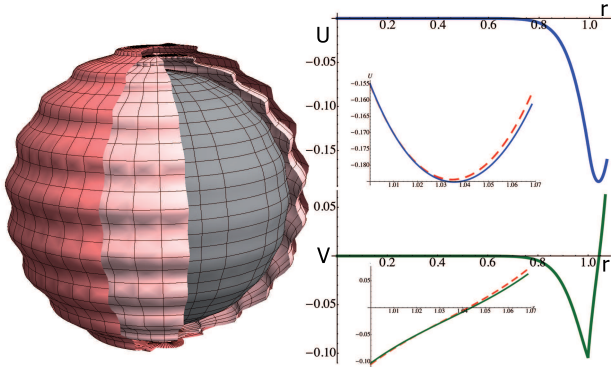

FIG. 4. (color online). Tumor morphology at the critical thresholds $g_s/g_c = 1.33$, $m = 20$ for $\mu^s/\mu^c = 1$, $R_o/R_i = 1.04$ (left). The numerical solutions (solid lines) and the WKB approximations (dashed lines) for the displacement fields U and V are shown setting $g_c R_i = 1$, and $\epsilon = 0.15$ (right).

Making iterations on the wavenumber and the aspect ratio, the control parameter g_s/g_c of the elastic bifurcation is obtained by integrating numerically Eq.(7) using the initial value $\mathbf{Z}^s(r_o) = \mathbf{0}$ and the stop condition $\det(\mathbf{Z}^d) = 0$, with $\mathbf{Z}^d = \mathbf{Z}^s(r_i) - \mathbf{Z}^c(r_i)$, corresponding to the continuity of the physical fields at the interface. An example of marginal stability curve for g_s/g_c is given in Fig. 2, with indication of the selected wavenumber of the instability. In particular, the critical thresholds g_s/g_c for the instability is barely constant for $R_o/R_i \geq 2$, with a selected wavenumber $m = 10$. For very thin tumor shells, i.e. $R_o/R_i \to 1$, a short-wavelength instability occurs ($m \to \infty$). In between these limits, the instability thresholds show a marked variability with the aspect ratio. In Fig. 3, the critical thresholds g_s/g_c are depicted in function of the shear moduli ratio μ^s/μ^c for different initial geometries of the tumor spheroid. A short wavelength buckling occurs in the rigid core limit, i.e. $\mu^s/\mu^c \to 0$, where a master curve $g_s/g_c = \beta \log(\mu^s/\mu^c)$ is found, with $\beta < 0$ being slope of the asymptotic line in the logarithmic plot. In general, the threshold values g_s/g_c decrease as the ratio μ^s/μ^c increase, albeit the selected wavelength strongly depends on the aspect ratio. Finally, the perturbed shape of the growing tumor spheroid can be obtained recalling that the ratio between the radial and the tangential displacements at r_i is given by the stop condition. In order to avoid numerical stiffness problems, the overall displacement and stress fields can be calculated by a successive numerical integration of the first of Eq.(6), being $d_r \mathbf{u}^s = \mathbf{N}_1 \mathbf{u}^s + \mathbf{N}_2 \mathbf{Z}^s \mathbf{u}^s$, with initial condition $\mathbf{u}^s(r_i) = \epsilon \left[-1, Z^d_{11}(r_i)/Z^d_{12}(r_i)\right]^T$, where ϵ is a small amplitude which cannot be fixed by a linear stability analysis. The morphology of a thin tumor spheroid at the instability threshold is depicted in Fig. 4, comparing the numerical solution with the WKB approximation of the strain fields. In general, the radial extension of the perturbation across the interface is found having a typical length of about $r_i \cdot 2\pi/m$.

In summary, a buckling instability may occur in tumor spheroids for the accumulation of residual solid stresses induced by the differential growth between the necrotic core and the outer shell of proliferative cells. The growth rate ratio g_s/g_c is the control parameter of this instability, depending both on the elastic and the geometric properties of the media. *This model provides clear-cut predictions on the onset of the instability that could be easily tested by performing in-vitro experiments on MCTS. Future developments will consider different boundary conditions, including an external elastic confinement for representing the compression of the healthy stroma during in-vivo tumor invasion.* The theoretical results suggest that the morphological transition driven by the residual stresses in tumors could be involved in triggering metastasis. Although the linear stability analysis fixes the thresholds and the wavelengths of the unstable wrinkling modes, the emerging three-dimensional pattern at the tumor surface will be driven by nonlinear effects. The post-buckling dynamics might promote tumor invasiveness through the formation of protrusions at the outer surface, which have been observed during collective migration of invasive cells and vascular sprouting [29].

This work is in part supported by EU grant ERG-256605, and by the NSF grant PHY05-51164. Dr. F. Acerbi (Istituto Besta, Milan) provided the clinical images in Fig. 1.

* Electronic address: pasquale.ciarletta@upmc.fr

[1] C.C. DuFort, M.J. Paszek, and V.M. Weaver. Nature Rev. Mol. Cell Biol. **12**, 308-319 (2011).

[2] D.E. Dicher, P. Jamney, and Y.L. Wang. Science **310**, 1139 (2005).
[3] B.I. Shraiman. Proc. Natl. Acad. Sci. USA **102**(9), 3318-3323 (2005).
[4] M.J. Paszek *et al.* Cancer Cell **8**,(2005) 241-254.
[5] S. Kumar, and V.M. Weaver. Cancer Matastasis Rev. **28**(1-2), 113-127 (2009).
[6] D. Wirtz, K. Kostantopoulos, and P.C. Searson. Nat. Rev. Cancer **11**, 512-522.
[7] H.B. Friboes *et al.* Cancer Res. **66**, 1597-1604 (2006).
[8] M. Ben Amar, C. Chatelain, and P. Ciarletta. Phys. Rev. Lett. **106**(14), 148101 (2011).
[9] T. Stylianopoulos *et al.* Proc. Natl. Acad. Sci. USA **109**(38), 15101-15108 (2012).
[10] P. Friedl, and K. Wolf. Nature Rev. Cancer **(**3), 362-373 (2003)
[11] A.L. Harris. Nature Rev. Cancer **(**2), 38-47 (2002)
[12] E.T. Roussos, J.S. Condeelis, and A. Patsialou. Nature Rev. Cancer **(**11), 573-587 (2011)
[13] J. Dervaux, and M. Ben Amar. Phys. Rev. Lett. **101**, 068101 (2008).
[14] E. Hannezo, J. Prost, and J.-F. Joanny. Phys. Rev. Lett. **107**(14), 078104 (2011).
[15] D.E. Moulton, and A. Goriely. J. Mech. Phys. Solids **59**, 525-537 (2011).
[16] M. Espinosa *et al.* Cancer Lett. **318**, 61-67 (2012).
[17] D. Gonzales-Rodriguez *et al.* Science **338**, 910 (2012)
[18] D. Ambrosi, and L. Preziosi. Biomech. Model. Mechanobiol. **8**, 397-413 (2009).
[19] G. Helmlinger *et al.* Nature Biotech. **15**, 778-783 (1997).
[20] P.A. Netti *et al.* Cancer Res. **60**, 2497-2503 (2000).
[21] J.P. Freyer, and R.M. Sutherland. Cancer Res. **46**, 3504-3512 (1986).
[22] E.K. Rodriguez, A. Hoger, and A. McCulloch. J. Biomech. **27**, 455-467 (1994).
[23] J. Ranft *et al.* Proc. Natl. Acad. Sci. USA **107**(49), 20863-20868 (2010).
[24] A.S. Wang, and A. Ertepinar. Int. J. Nonlinear Mech. **7**, 539-555 (1972).
[25] A. Goriely, and M. Ben Amar. Phys. Rev. Lett. **94**, 198103 (2005).
[26] A.N. Norris, and A. L. Shuvalov. Proc. R. Soc. A **468**, 467-484 (2012).
[27] B. Li *et al.* Phys. Rev. Lett. **106**, 234301 (2011).
[28] M. Destrade, A. Ní Annaidh, and C.D. Coman. Int. J. Solids Struct. **46**, 4322-4330 (2009).
[29] J.M. Tse *et al.* Proc. Natl. Acad. Sci. USA **109**(3), 911-916 (2012).